Influence of Exciton Dimensionality on Spectral Diffusion of Single-Walled Carbon Nanotubes

Xuedan Ma,*,† Oleksiy Roslyak,†,‡ Feng Wang,† Juan G. Duque,§ Andrei Piryatinski,‡ Stephen K. Doorn,† and Han Htoon*,†

†Center for Integrated Nanotechnologies, Materials Physics and Applications Division, ‡Theoretical Division, and §Physical Chemistry and Applied Spectroscopy Group, Chemistry Division, Los Alamos National Laboratory, Los Alamos, New Mexico 87545, United States

ABSTRACT We study temporal evolution of photoluminescence (PL) spectra from individual single-walled carbon nanotubes (SWCNTs) at cryogenic and room temperatures. Sublinear and superlinear correlations between fluctuating PL spectral positions and line widths are observed at cryogenic and room temperatures, respectively. We develop a simple model to explain these two different spectral diffusion behaviors in the framework of quantum-confined Stark effect (QCSE) caused by surface charges trapped in the vicinity of SWCNTs. We show that the wave function properties of excitons, namely, localization at cryogenic temperature and delocalization at room temperature, play a critical role in defining sub- and superlinear correlations. Room temperature PL spectral positions and line widths of SWCNTs coupled to gold dimer nanoantennas on the other hand exhibit sublinear correlations, indicating that excitonic emission mainly originates from nanometer range regions and excitons appear to be localized. Our numerical simulations show that such apparent localization of excitons results from plasmonic confinement of excitation and an enhancement of decay rates in the gap of the dimer nanoantennas.

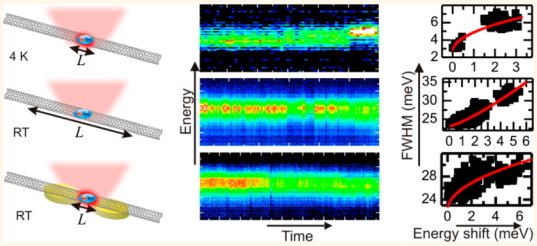

KEYWORDS: carbon nanotubes · quantum-confined Stark effect · surface plasmons · photoluminescence · spectral diffusion

Semiconducting single-walled carbon nanotubes (SWCNTs) are quasi-one-dimensional (1D) nanostructures where strongly correlated electron–hole pairs with binding energies of up to several hundred meV[1] are confined in one dimension. Because of their photoluminescence (PL) emission that spans over the 1.3–1.5 μm telecom spectral regime and recent demonstration of strong photon antibunching at cryogenic temperature,[2] individual SWCNTs have been considered as an ideal candidate for single photon sources that are needed for realization of quantum information processing.[3] However, such an application also demands indistinguishable single photons with ideal spectral purity.[4,5] Although several groups have reported observation of PL spectra with ultranarrow line width and free of spectral diffusion from suspended SWCNTs at cryogenic temperatures,[6,7] realization of such quality in individual SWCNTs at room temperature or in those wrapped with surfactants is currently difficult because their PL exhibits spectral diffusion, which manifests itself either as random wandering of spectral lines and/or inhomogeneous broadening.[3,8−10] While spectral diffusion has been commonly attributed to strong environmental interactions derived from the single layer structure of SWCNTs,[11,12] a detailed understanding of the responsible physical mechanism is still lacking. Such an understanding is highly desirable for optimization of SWCNTs toward single photon source applications.

Spectral diffusion has also been observed in semiconducting quantum dots (QDs),[13] quantum rods,[14,15] and gold nanoclusters,[16] and it is commonly attributed to quantum-confined Stark effect (QCSE) caused by fluctuations of local surface charges. Specifically, surface charges on nanostructures can create a local electric field that can increase exciton binding energy and consequently decrease the effective bandgap.[17] While fluctuations of such a local electric field happening at time scales larger than the experimental integration time lead to a shift of peak position, fast fluctuations

* Address correspondence to xma@lanl.gov, htoon@lanl.gov.

Received for review July 25, 2014 and accepted September 24, 2014.

Published online September 24, 2014
10.1021/nn504138m

contribute to spectral broadening since it cannot be resolved during the experimental integration time. In the case of 0D QDs, such spectral diffusion-induced broadening dominates in defining spectral line widths, yielding a quadratic relation between spectral broadening and peak red-shift.[14,18−20] Although these interesting effects of QCSE have been investigated thoroughly in QDs, study of spectral diffusion behavior in SWCNTs in this context is quite limited. Specifically, while a quadratic relation between spectral broadening and peak red-shift has been reported in low temperature PL study of SWCNTs,[8] how this behavior would evolve as a function of external influences such as sample temperature and local plasmonic effect has never been investigated.

Unlike 0D QDs, excitons of SWCNTs can demonstrate both 0D and 1D characteristics depending on experimental conditions. For example, while excitons of SWCNTs can diffuse along the tube over hundreds of nanometers at room temperature,[21] they tend to localize to QD-like states at cryogenic temperatures.[2] Moreover, recent experimental[22] and theoretical[23] studies have shown that coupling SWCNTs to localized surface plasmons can modify their radiation rate and pattern in such a way that tube emission mainly originates from the interaction region. Because of excitons' 1D diffusive nature under certain environments, a change of exciton position can dominate over the fluctuation of surface charges/dielectric environments in defining the local electric field fluctuation. 0D to 1D transition of excitons can therefore have strong influence on the spectral diffusion behavior of SWCNTs. A detailed understanding of such influence is essential to achieve effective control of emission properties of SWCNTs in different environments. In addition, the study of spectral diffusion behavior of SWCNTs coupled to metallic nanostructures can in turn help us understand the complex interactions between 1D excitons and surface plasmons.

Here, we study temporal evolution of photoluminescence (PL) spectra from individual SWCNTs both at low and room temperatures. By correlating the PL spectral position and line width, we can assign the observed spectral diffusion to quantum-confined Stark effect (QCSE) caused by surface charges located in the vicinity of the SWCNTs. By applying a simple point charge model, we reveal that the differences observed for the low and room temperature QCSE in SWCNTs can be explained by the different wave function properties of excitons at different temperatures. We further apply this method to SWCNTs coupled to gold nanoantennas, and demonstrate that their room temperature PL spectral position and line width exhibit a sublinear correlation, indicating that excitonic emission mainly originates from nanometer scale regions and excitons appear to be localized. Numerical simulations reveal that such "localization" results from strong

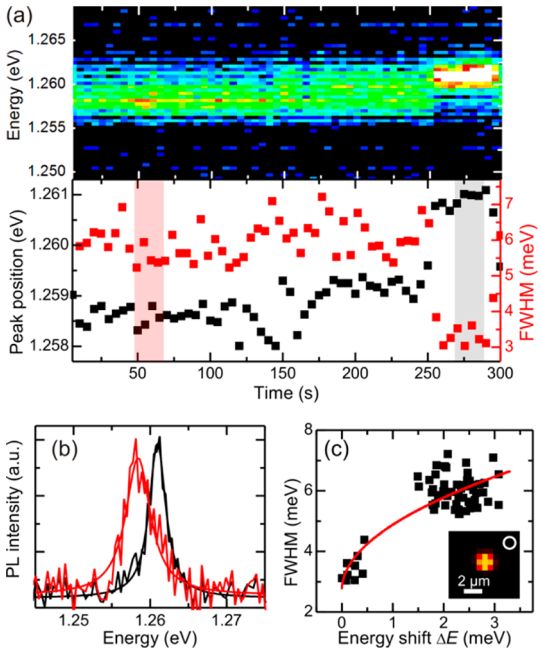

Figure 1. (a) Temporal evolution of PL spectra of an individual SWCNT measured at 5 K (upper panel) together with the corresponding PL peak position (black) and line width (red) (lower panel) extracted from Lorentzian fittings. The integration time per spectrum is 5 s. (b) Two PL spectra of the tube extracted from the marked time regions in (a) (lower panel) fitted with Lorentzian functions. (c) Correlation between peak redshift ΔE and peak line width extracted from the time trace of spectra in (a). Sublinear correlations can be observed. The red curve is a fitting to $(\Delta E)^{1/2}$. Inset is a wide-field PL image of the tube, and for comparison, the white circle denotes the laser spot size in the confocal mode.

confinement of excitation and enhancement of decay rates in the gaps of the nanoantennas where excitons interact strongly with surface plasmons. Our study not only has a strong implication toward understanding the local electrostatic environment of SWCNTs and provides useful information for fabrication of samples free of spectral-diffusion, but also introduces a simple method for determining the wave function properties of excitons in different environments.

RESULTS AND DISCUSSION

To monitor spectral diffusion of individual SWCNTs, we measure time traces of PL spectra by confocally exciting SWCNTs at their center. Figure 1a (upper panel) shows temporal evolution of PL spectra from an individual SWCNT at 5 K. Virtually constant PL intensity and peak position can be observed between 0−250 s, followed by a sudden spectral jump to the blue accompanying an increase in the PL intensity. To quantitatively analyze these spectra, we applied a Lorentzian fit to each spectrum and extracted the time-dependent peak position and full width at half-maximum (fwhm) values (Figure 1a lower panel). Relative fitting errors for both values were determined to be <5.0%. The spectral line widths of 3−7 meV are

close to previously reported low temperature results.[24,25] Significant spectral narrowing together with a peak blue shift can be observed at 250 s. Figure 1b shows two spectra of the SWCNT extracted from the marked time regions in Figure 1a (lower panel). Fitting the two spectra with Lorentzian functions gives peak positions of 1.261 eV ± 0.0662 meV (black) and 1.258 eV ± 0.139 meV (red), and fwhm values of 2.61 ± 0.0194 meV (black) and 3.92 ± 0.0414 meV (red), respectively, indicating the red-shifted spectrum of the two is much broader than the blue-shifted one.

Similar spectral behavior attributed to QCSE has been observed in 0D quantum emitters,[13−16] and it is not surprising to observe this kind of spectral behavior in SWCNTs at cryogenic temperature because localized, quantum-dot like excitonic states due to disorder tend to form at this temperature.[2] The wide-field PL image in Figure 1c, where emission from the SWCNT is diffraction limited, which is typically observed in our experiment at this temperature (see Supporting Information S1) and also previously reported by other studies,[2] further supports this scenario. With anionic surfactants (SDBS in this case) on SWCNT surface serving as possible negative charge sources,[26,27] it is reasonable to conclude that change from the red-shifted, low intensity emission in Figure 1a (0−250 s) to the blue-shifted, high intensity emission (Figure 1a, 250−300 s) is due to fluctuation of local electric field.

We then studied spectral diffusion of SWCNTs at room temperature to understand the influence of QCSE on diffusive 1D excitons.[21,28,29] Figure 2c inset shows a wide-field PL image of an individual SWCNT at room temperature. Different from diffraction-limited emission at low temperature (Figure 1c inset), elongated emission along the tube can be observed. Figure 2a (upper panel) shows temporal evolution of PL spectra from the individual SWCNT at room temperature. Compared to low temperature, more PL fluctuation can be observed. Again, by fitting each spectrum with a Lorentzian function, PL peak position and line width (Figure 2a, lower panel) can be extracted. Relative fitting errors for both values were determined to be <4.5%. Figure 2b shows two representative PL spectra of the SWCNT extracted from the marked time regions in Figure 2a (lower panel). Fitting the two spectra with Lorentzian functions gives peak positions of 1.250 eV ± 0.270 meV (black) and 1.254 eV ± 0.131 meV, and fwhm values of 30.38 ± 1.22 meV (black) and 24.00 ± 0.0528 meV (red), respectively. Similar to low temperature spectra, a red shift in peak position is correlated to spectral broadening, indicating the existence of QCSE. Additionally, from Figure 2a we can observe that PL blinking is oftentimes followed by a large spectral shift (*e.g.*, at 215 and 700 s). This phenomenon is consistent with the above-mentioned QCSE involving local electric field fluctuation.[30]

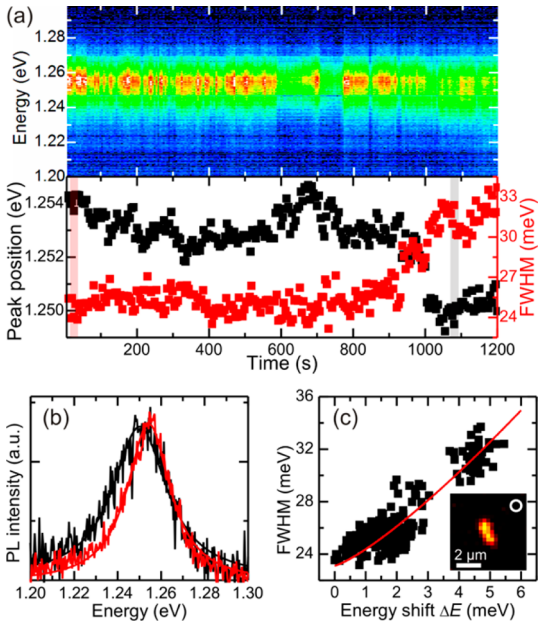

Figure 2. (a) Temporal evolution of PL spectra of an individual SWCNT measured at room temperature (upper panel) together with the corresponding PL peak position (black) and line width (red) (lower panel) extracted from Lorentzian fittings. Integration time per spectrum is 5 s. (b) Two PL spectra of the tube extracted from the marked time regions in (a) (lower panel) fitted with Lorentzian functions. (c) Correlation between peak redshift ΔE and peak line width extracted from the time trace of spectra in (a). Superlinear correlations can be observed. The red curve is a fitting to $\Delta E^{5/4}$. Inset is a wide-field PL image of the tube, and for comparison, the white circle denotes laser spot size in the confocal mode.

Our room temperature spectral diffusion study of SWCNTs indicates that even if the exciton is diffusive, it is still under the influence of QCSE. However, despite the existence of QCSE at both cryogenic and room temperatures, the detailed interaction mechanism between exciton and surface charge should be different. At cryogenic temperature, excitons are localized to quantum-dot like states, leading to fixed exciton-charge distance. Additionally, it is also reasonable to assume that the local dielectric environment surrounding the localized exciton at cryogenic temperature is stable. Therefore, spectral diffusion is mainly induced by surface charge fluctuation, same as in the case of QDs.[18] However, at room temperature, both exciton diffusion and surface charge/dielectric environment fluctuation can affect spectral diffusion. To be more specific, according to both theoretical calculation[17] and experimental measurements,[18,31] to generate a spectral redshift of ~10 meV, an electric field on the order of 10^5 V/cm is needed, which can be created by a single electron at the distance of ~12 nm from the exciton. On the other hand, for a 1D exciton diffusing over hundreds of nanometers along the tube, the fluctuation of distance between the exciton and surface charge can lead to orders of magnitude fluctuation in electric field, causing from a fraction of a meV

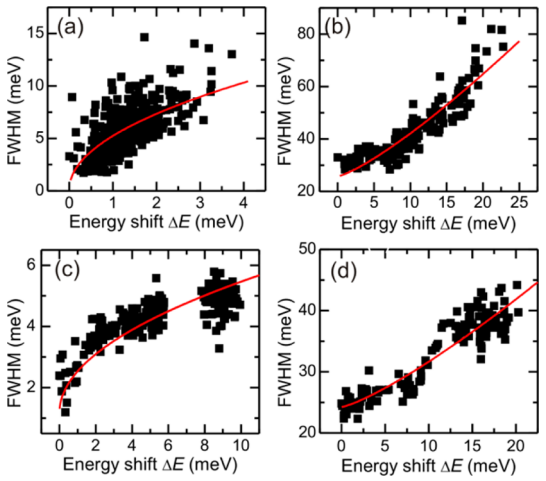

Figure 3. Correlation between peak redshift ΔE and peak line width from (a, c) two individual SWCNTs at 4.2 K, and (b, d) two individual SWCNTs at room temperature, respectively. Sublinear and superlinear correlations can be observed at 4.2 K (a, c) and room temperature (b, d), respectively. Red curves are fittings to (a, c) $(\Delta E)^{1/2}$ and (b, d) $\Delta E^{5/4}$.

to tens of meV spectral shift. This fluctuation can dominate over the local surface charge/dielectric environment fluctuation. Therefore, exciton diffusion has significant influence on the spectral diffusion of SWCNTs. To elucidate this influence, we take the peak position of the bluest spectrum recorded for each SWCNT as a reference, and peak redshift is plotted against peak line width in Figure 1c and 2c. Interestingly, for SWCNTs at low temperature (Figure 1c), a sublinear correlation between the peak redshift and line width is observed, while for tubes measured at room temperature (Figure 2c), a superlinear correlation can be found. Such behavior is commonly observed in our experiments (70% of tubes for low temperature and 75% for room temperature. See Figure 3 for more examples and Supporting Information S2 for histograms of correlation coefficients). In the following we discuss in detail how this significant difference can be explained by the different nature of exciton wave function properties of SWCNTs at different temperatures, *i.e.*, localization at cryogenic temperature and delocalization at room temperature.

We use a simple point charge model in the framework of QCSE to explain the observed difference. For SWCNTs at low electric field, an energy shift of the binding energy (ΔE) caused by QCSE can be described by[17]

$$\Delta E = k_b \frac{(edF)^2}{E} \tag{1}$$

where e is the electron charge, d the tube diameter, E the tube binding energy at zero field, F the electric field induced by surface charges, and k_b a constant. If we use a Gaussian stochastic model to describe spectral diffusion behavior: $\langle \delta(\Delta E)(t)\delta(\Delta E)(0)\rangle = \sigma^2 e^{-t/t_c}$, with σ being the Gaussian full-width at half-maximum (*i.e.*, spectral broadening in meV) and t_c the correlation time, at $t = 0$ we obtain[32]

$$\langle \delta^2(\Delta E)(0)\rangle = \sigma^2 \tag{2}$$

We then assume that there is an external point charge q located on the surface of a SWCNT that creates a local electric field $F = (q/(4\pi\varepsilon r^2))$, with ε being the permittivity of the surrounding environment and r the exciton-charge distance. Here, a single point charge is chosen for the sake of clarity. More realistic geometries of multiple charges can be used but do not alter the conclusions. In order to calculate spectral broadening σ as a function of binding energy shift ΔE, we consider two temperature regimes. At low temperature, since an exciton in SWCNT tends to localize to quantum-dot-like states, exciton-charge distance r and local environment permittivity ε can be considered to be constant and hence, local electric field fluctuation (δF) is mainly induced by fluctuations in surface charges (δq):

$$\delta F = \frac{1}{4\pi\varepsilon r^2}\delta q \tag{3}$$

On the basis of these assumptions, we obtain (see Supporting Information S4 for details)

$$\sigma \propto \sqrt{\Delta E}\langle \delta^2 q\rangle^{1/2} \tag{4}$$

with $\langle \delta^2 q\rangle^{1/2}$ being our fitting parameter. In fact, data points in Figures 1c, 3a and 3c can be fit reasonably well (red curves) by this correlation with relative standard errors <10.4%. Increasing the integration time from 5 to 15 s has no significant influence on the fitting result (Supporting Information S3). In contrast, at room temperature, excitons can diffuse freely along the tube, leading to a large fluctuation in exciton-charge distance r and consequently binding energy, while contributions of surface charge/dielectric environment fluctuation become negligible. Therefore, local environment permittivity ε and surface charge q can be taken as constants, and fluctuation of local electric field is

$$\delta F = -\frac{2q}{4\pi\varepsilon r^3}\delta r \tag{5}$$

From $F = (q/(4\pi\varepsilon r^2))$ we have $(1/r^3) = ((4\pi\varepsilon F)/q)^{3/2}$. Therefore, eq 5 becomes

$$\delta F = -\frac{2(4\pi)^{1/2}\varepsilon^{1/2}F^{3/2}}{q^{1/2}}\delta r \tag{6}$$

From eqs 1, 2 and 6, we can then get (see Supporting Information S4 for details)

$$\sigma \propto \Delta E^{5/4}\langle \delta^2 r\rangle^{1/2} \tag{7}$$

with $\langle \delta^2 r\rangle^{1/2}$ being our fitting parameter. Fitting data points in Figures 2c, 3b, and 3d with eq 7 (red curve) shows very good agreement (relative standard error <3.80%). Additionally, spectral-diffusion free line widths

at $\Delta E = 0$ derived from the fittings are 23.1 meV (Figure 2c), 25.7 meV (Figure 3b), and 24.2 meV (Figure 3d), respectively, in reasonable agreement with reported room temperature line widths of SWCNTs resulted from exciton−phonon coupling.[33,34]

Having established the origin of spectral diffusion in SWCNT as QCSE and its relation to exciton wave function properties in different environments, we now apply this method on SWCNTs coupled to surface plasmons at room temperature. Böhmler *et al.*,[22] using a sharp gold tip positioned at ~4 nm distance from a SWCNT, showed that when the gold tip approached the SWCNT, energy from the tube was transferred to the tip through near-field interaction, modifying the radiation pattern of the nanotube. Roslyak *et al.*,[23] using a general theoretical approach, further confirmed the influence of exciton-surface plasmon interaction on the shape of the radiation pattern and exciton decay rates. These studies point to the possibility of exciton-surface plasmon interaction induced modification in the spectral diffusion behavior of SWCNTs.

Figure 4a shows a wide-field PL image of a SWCNT deposited on gold dimer nanoantenna arrays at room temperature. The horizontal lines are due to imperfect blocking of stray light scattered by the nanoantennas. Figure 4b shows a scanning electron microscope image of an area of the nanoantenna arrays. It can be seen that when the SWCNT is coupled to the nanoantennas (*e.g.*, Figure 4a, white circle), PL emission becomes localized and much brighter compared to that on the substrate. Such surface plasmon assisted PL enhancement of SWCNTs has been reported in previous studies.[35,36] We record room temperature temporal evolution of PL spectra from the spot marked in Figure 4a, and fit each spectrum with a Lorentzian function to extract peak position and line width, as shown in Figure 4c. Similar to SWCNTs on quartz substrates, peak redshift is correlated to spectral broadening. We then plot the line width-peak redshift correlation in Figure 4d, and the data points can be well fitted with eq 4 (red curve) with relative standard error <7.8%. This $\sigma \propto (\Delta E)^{1/2}$ correlation is similar to what we observed for SWCNTs at low temperature (Figures 1c, 3a, and 3c), and indicates that for SWCNTs coupled to surface plasmons, excitonic emission mainly originates from the coupling region and excitons appear to be "localized", consistent with the PL image in Figure 4a. However, it is worth mentioning that different from the case of carbon nanotubes at low temperature, where excitons are localized to 0D quantum-dot like excitonic states, the wave function properties of the carbon nanotubes coupled to gold nanoantennas at room temperature remain 1D. To distinguish this kind of exciton "localization" at room temperature due to a spatial narrowing of the recombination region from the real wave function localization happening at low

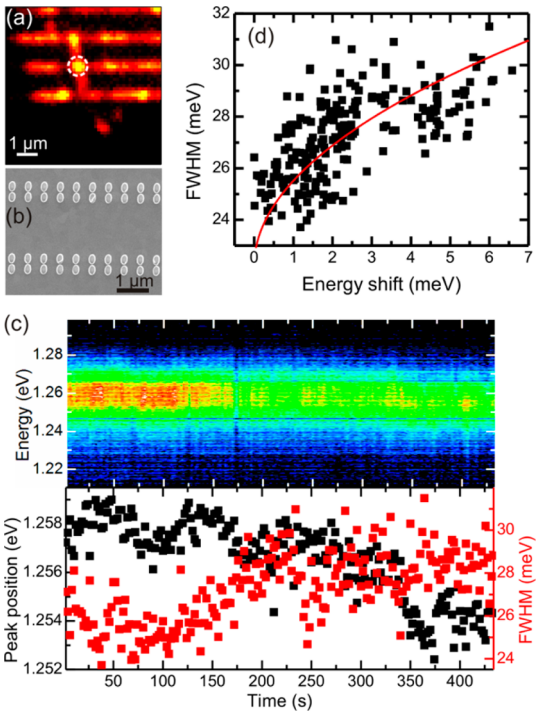

Figure 4. (a) A wide-field PL image of a SWCNT deposited on gold nanoantenna arrays measured at room temperature. The white circle denotes laser spot size in the confocal mode. The horizontal lines are stray lights scattered by the nanoantennas. Bright and localized emission from segments of the SWCNT coupled to the nanoantennas can be observed. (b) A scanning electron microscopy image of an area from the gold nanoantenna arrays. The orientation of the nanoantenna arrays is adjusted to be the same as in (a). (c) Room temperature temporal evolution of PL spectra of the SWCNT marked in (a) (upper panel) together with the corresponding PL peak position (black) and line width (red) (lower panel) extracted from Lorentzian fittings. Integration time per spectrum is 2 s. (d) Correlation between peak redshift and line width from PL spectra of the SWCNT coupled to gold nanoantennas. The red curve is a fitting to $(\Delta E)^{1/2}$.

temperature, we describe the former as the "apparent localization" of excitons.

To further elucidate the reason for this apparent exciton localization in SWCNTs, we numerically simulate the system of SWCNTs coupled to gold dimer nanoantennas. Figure 5a inset shows the configuration of the simulated system consisting of two Au nanoantennas aligned along their long radius. To calculate the extinction spectrum with the three-dimensional finite-difference time-domain (3D FDTD) method, we assume a plane wave propagating perpendicularly down (-*z* direction) toward the nanoantennas. Since only the transverse mode (~2.15 eV), which is off-resonance with SWCNT emission (~1.25 eV) and excitation (1.53 eV) energies, can be excited when the plane wave is polarized along the *y*-axis, this excitation geometry will only have a negligible influence on the PL of SWCNTs. Therefore, in the following we will focus our discussion on the situation when the plane wave is polarized along the *x*-axis. Figure 5a shows the simulated

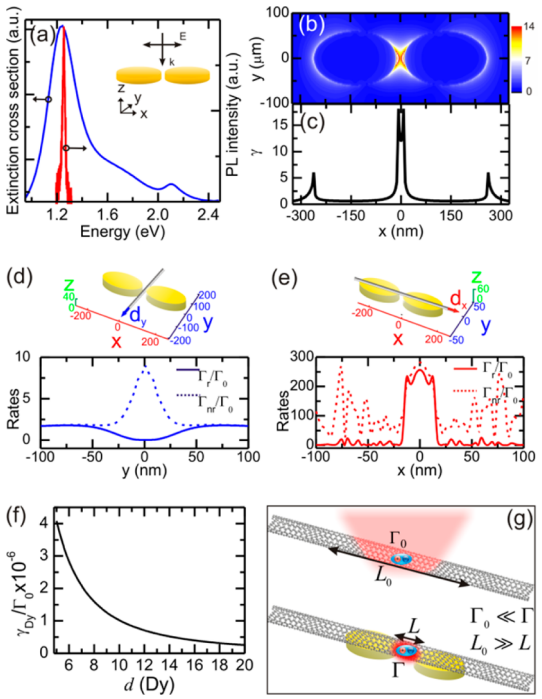

Figure 5. (a) Simulated extinction spectrum (blue curve) together with a PL spectrum of a SWCNT (red curve) measured at room temperature. Inset: configuration of the simulated system consisting of two nanoantennas. A plane wave polarized along the *x*-axis with energy in the range of 0.95 and 2.48 eV propagates perpendicularly toward the nanoantennas. Dimensions of the dimer nanoantennas are measured from scanning electron microscope images. Length, width and height of each nanoantenna are 250, 120, and 48 nm, respectively. Gap distance between two adjacent dimer nanoantennas is 20 nm. (b) Contour plot of the simulated local electric field enhancement factor close to the gold dimer nanoantennas. (c) Field enhancement factor γ along the center axes ($y = 0$) of the nanoantennas. (d, e) Radiative and nonradiative decay rates of an exciton as a function of the dipole position along the SWCNT. Γ_0 is the exciton decay rate without the presence of metal. (f) Dissipation rate of excitons in gold (γ_{Dy}) in the form of Ohmic losses as a function of SWCNT exciton dipole moments (*d*). (g) A sketch of excitons in SWCNTs with (lower) and without (upper) coupling to Au dimer nanoantennas. While the decay rate of excitons coupled to surface plasmon (Γ) is much larger than that of free-standing excitons (Γ_0), the average diffusing distance of excitons coupled to surface plasmon (L) is much smaller than that of free-standing excitons (L_0).

extinction spectrum (blue curve) together with a representative PL spectrum of the studied SWCNTs measured at room temperature (red curve), and it can be seen that the longitudinal surface plasmon mode (~1.24 eV) from the dimer nanoantennas is in good resonance with the PL of the SWCNTs. We also simulate the local electric field enhancement factor γ, which is defined as the ratio of the electric field intensity at the excitation wavelength (810 nm) with and without the gold dimer nanoantennas present with the 3D FDTD method, and the simulation result is shown in Figure 5b. Obviously, the local electric field intensity is strongly dependent on the relative location of the SWCNTs.[35] The field enhancement factor γ along the center axes of the nanoantennas is plotted in Figure 5c. A γ value larger than 15 can be observed between the dimer gap in a range smaller than 30 nm. Since the excitation rate is proportional to the local electric field at the position of the emitter,[37] such strong enhancement of the electric field in-between the dimer gap can consequently lead to significantly confined excitation in that region.

We further simulate the influences of surface plasmons on the decay rate of the excitons with a general theoretical approach (see Supporting Information S5 for details). Figure 5d and 5e show the radiative and nonradiative rates of an exciton as a function of the dipole position along the SWCNT. In the first approximation, we assume the oscillator strength of the dipole oriented perpendicular to the tube is negligible and only that oriented parallel to the tube is considered. When the SWCNT is in the middle of the Au dimer nanoantennas and aligned perpendicular to their long axes (Figure 5d), an increase in the nonradiative rate and a decrease in the radiative rate can be expected for the segment of SWCNT in-between the dimer, indicating a reduction in the PL intensity. However, when the tube is placed right on top of the dimer and aligned along their long axes (Figure 5e), significant enhancements both in the radiative and nonradiative rates can be observed for the segment of SWCNT in-between the dimer. Such enhancement in the decay rates may be responsible for the brighter PL emission observed in Figure 4a. Outside the coupling region, the nonradiative rate dominates because energy transferred to the metal is fully lost into Ohmic heat. Figure 5f shows the dissipation rate of excitons (γ_{Dy}) in gold in the form of Ohmic losses for possible values of SWCNT exciton dipole moments. The value of Γ_0/γ_{Dy}, with Γ_0 being the exciton decay rate without the presence of metal, is $\sim 10^{-6}$, indicating the studied system corresponds to the weak coupling regime, and energy transfers one-way from SWCNT exciton to surface plasmons. Such one-way transfer of energy is the reason for the significant enhancement in the nonradiative rate of the tubes. Overall, from Figure 5d and 5e, the total decay rate of SWCNTs coupled to dimer nanoantennas can be enhanced by factors of 10−500. If we take the diffusion length of the tubes without coupling to the nanoantennas as 90 nm from ref 21, plasmonic coupling of the tubes can reduce the diffusion length to ~4−28 nm. In agreement with our simulation results, Böhmler *et al.*[22] showed that when a gold tip approached a SWCNT, energy from the tube was transferred to the tip through near-field interaction, and without taking into account the changes in nonradiative decay rate, an enhancement factor of the radiative decay rate as large as 13.6 was observed.

On the basis of the above simulation results, we can interpolate the reason for the apparent exciton localization in SWCNTs coupled to localized surface

plasmons with the sketch in Figure 5g. On one hand, as we can see from Figure 5b and 5c, the gold nanoantennas can focus the incident beam to a region that is far below the diffraction limit. Since optical excitation rate is proportional to the local electric field intensity, this kind of optical confinement effect[38,39] leads to excitation of a SWCNT mainly in a small subdiffraction segment (<30 nm) that is in the gap of the dimer nanoantennas. On the other hand, once the segment of the SWCNT in-between the dimer nanoantennas is excited, the generated excitons can decay much faster compared to the situation without the nearby nanoantennas. Consequently, the chance of an exciton diffusing away from the excitation spot is significantly reduced. Therefore, both the highly confined excitation and enhanced decay rate indicate that excitons coupled to strongly localized surface plasmons tend to appear localized because the chance of exciton diffusion is significantly reduced by these two effects.

CONCLUSIONS

In conclusion, we study spectral diffusion in SWCNTs by means of monitoring time traces of the PL spectrum. Correlation between PL peak position and line width can be observed for SWCNTs both at cryogenic and room temperatures, which we attribute to QCSE induced by surface charges in the vicinity of SWCNTs. However, while tubes at low temperature exhibit sublinear correlation between peak position and line width, those at room temperature show superlinear correlation. We explain this difference with a simple point charge model based on the QCSE, and reveal that the difference is due to the different exciton wave function properties of SWCNTs at different temperatures: while localization of an exciton at low temperature leads to a sublinear correlation between PL peak position and line width, free diffusion of exciton at room temperature results in a superlinear correlation. We further apply this method to SWCNTs coupled to gold dimer nanoantennas at room temperature, and demonstrate that effective exciton−plasmon interaction changes the diffusion behavior of SWCNT excitons and leads to their apparent localization. Our numerical simulations indicate that highly confined excitation and enhanced decay rates are the factors contributing to such apparent exciton localization. Our finding has important implication toward understanding the local electrostatic environments of SWCNTs and hence the physical mechanism in spectral diffusion of SWCNTs. Moreover, we provide a simple method for determining the exciton wave function properties of SWCNTs in different environments.

MATERIALS AND METHODS

SWCNTs used in this study were prepared by mild sonication of HiPco material in a 1% aqueous solution of sodium dodecyl benzenesulfonate (SDBS) followed by chirality sorting using the nonlinear density gradient ultracentrifugation method.[40,41] Suspension fractions enriched in (6,5) tubes were collected and stored for PL experiments. Gold dimer nanoantenna arrays[42,43] with gap size smaller than 20 nm and longitudinal surface plasmon mode at ~1.24 eV were fabricated by electron beam lithography on indium tin oxide (ITO) substrates. Each dimer nanoantenna is composed of a pair of ellipses with length, width and height of 250, 120, and 48 nm, respectively. To prepare samples for individual SWCNT PL measurements, a 5−10 μL drop of nanotube suspension was deposited on a precleaned quartz or a fabricated ITO substrate. Density of the tubes was controlled to be smaller than one tube per 10 × 10 μm^2 area. Single tube PL measurements were performed on a home-built confocal laser microscope. A continuous-wave Ti-Sapphire laser operating at 810 nm (1.53 eV) was used to excite (6,5) SWCNTs at their E_{11} phonon sideband. For low temperature experiments, samples were mounted in a continuous-flow, liquid-He cryostat with a 4.2 K base temperature. Microscope objectives were used to focus laser beam and collect PL signals. Spectral emission from the sample was dispersed using a 0.3 m spectrograph and imaged by a 2D InGaAs array. The excitation power was kept low enough to exclude exciton−exciton interactions.

Conflict of Interest: The authors declare no competing financial interest.

Acknowledgment. This work was conducted at the Center for Integrated Nanotechnologies (CINT), a U.S. Department of Energy, Office of Basic Energy Sciences (OBES) user facility and supported in part by Los Alamos National Laboratory Directed Research and Development Funds.

Supporting Information Available: Photoluminescence images at cryogenic and room temperatures; Histograms of correlation coefficients; Influence of integration time on the correlation between spectral shift and broadening; Theoretical method for calculation of correlation between spectral shift and line width; theoretical method for simulation of exciton decay rates in SWCNTs coupled to surface plasmons. This material is available free of charge *via* the Internet at http://pubs.acs.org.

REFERENCES AND NOTES

1. Maultzsch, J.; Pomraenke, R.; Reich, S.; Chang, E.; Prezzi, D.; Ruini, A.; Molinari, E.; Strano, M. S.; Thomsen, C.; Lienau, C. Exciton Binding Energies in Carbon Nanotubes from Two-Photon Photoluminescence. *Phys. Rev. B: Condens. Matter Mater. Phys.* **2005**, *72*, 241402.
2. Hoegele, A.; Galland, C.; Winger, M.; Imamoglu, A. Photon Antibunching in the Photoluminescence Spectra of a Single Carbon Nanotube. *Phys. Rev. Lett.* **2008**, *100*, 217401.
3. Walden-Newman, W.; Sarpkaya, I.; Strauf, S. Quantum Light Signatures and Nanosecond Spectral Diffusion from Cavity-Embedded Carbon Nanotubes. *Nano Lett.* **2012**, *12*, 1934–1941.
4. Knill, E.; Laflamme, R.; Milburn, G. J. A Scheme for Efficient Quantum Computation with Linear Optics. *Nature* **2001**, *409*, 46–52.
5. O'Brien, J. L.; Furusawa, A.; Vuckovic, J. Photonic Quantum Technologies. *Nat. Photonics* **2009**, *3*, 687–695.
6. Hofmann, M. S.; Glueckert, J. T.; Noe, J.; Bourjau, C.; Dehmel, R.; Hoegele, A. Bright, Long-Lived and Coherent Excitons in Carbon Nanotube Quantum Dots. *Nat. Nanotechnol.* **2013**, *8*, 502–505.
7. Sarpkaya, I.; Zhang, Z.; Walden-Newman, W.; Wang, X.; Hone, J.; Wong, C. W.; Strauf, S. Prolonged Spontaneous Emission and Dephasing of Localized Excitons in Air-Bridged Carbon Nanotubes. *Nat. Commun.* **2013**, *4*, 2152.

8. Matsuda, K.; Inoue, T.; Murakami, Y.; Maruyama, S.; Kanemitsu, Y. Exciton Fine Structure in a Single Carbon Nanotube Revealed Through Spectral Diffusion. *Phys. Rev. B: Condens. Matter Mater. Phys.* **2008**, *77*, 193405.
9. Matsuda, K.; Kanemitsu, Y.; Irie, K.; Saiki, T.; Someya, T.; Miyauchi, T.; Maruyama, S. Photoluminescence Intermittency in an Individual Single-Walled Carbon Nanotube at Room Temperature. *Appl. Phys. Lett.* **2005**, *86*, 123116.
10. Vialla, F.; Chassagneux, Y.; Ferreira, R.; Roquelet, C.; Diederichs, C.; Cassabois, G.; Roussignol, Ph.; Lauret, J. S.; Voisin, C. Unifying the Low-Temperature Photoluminescence Spectra of Carbon Nanotubes: The Role of Acoustic Phonon Confinement. *Phys. Rev. Lett.* **2014**, *113*, 057402.
11. Tsyboulski, D. A.; Bachilo, S. M.; Weisman, R. B. Versatile Visualization of Individual Single-Walled Carbon Nanotubes with Near-Infrared Fluorescence Microscopy. *Nano Lett.* **2005**, *5*, 975–979.
12. Ai, N.; Walden-Newman, W.; Song, Q.; Kalliakos, S.; Strauf, S. Pure Optical Dephasing Dynamics in Semiconducting Single-Walled Carbon Nanotubes. *ACS Nano* **2011**, *5*, 2664–2670.
13. Gomez, D. E.; Embden, J. van; Mulvaney, P. Spectral Diffusion of Single Semiconductor Nanocrystals: The Influence of the Dielectric Environment. *Appl. Phys. Lett.* **2006**, *88*, 154106.
14. Mueller, J.; Lupton, J. M.; Rogen, A. L.; Feldmann, J.; Talapin, D. V.; Weller, H. Monitoring Surface Charge Movement in Single Elongated Semiconductor Nanocrystals. *Phys. Rev. Lett.* **2004**, *93*, 167402.
15. Rothenberg, E.; Kazes, M.; Shaviv, E.; Banin, U. Electric Field Induced Switching of the Fluorescence of Single Semiconductor Quantum Rods. *Nano Lett.* **2005**, *5*, 1581–1586.
16. Wen, X.; Yu, P.; Toh, Y.-R.; Tang, J. Quantum Confined Stark Effect in Au_8 and Au_{25} Nanoclusters. *J. Phys. Chem. C* **2013**, *117*, 3621–3626.
17. Perebeinos, V.; Avouris, P. Exciton Ionization, Franz-Keldysh, and Stark Effects in Carbon Nanotubes. *Nano Lett.* **2007**, *7*, 609–613.
18. Empedocles, S. A.; Bawendi, M. G. Quantum-Confined Stark Effect in Single CdSe Nanocrystallite Quantum Dots. *Science* **1997**, *278*, 2114–2117.
19. Seufert, J.; Obert, M.; Scheibner, M.; Gippius, N. A.; Bacher, G.; Forchel, A.; Passow, T.; Leonardi, K.; Hommel, D. Stark Effect and Polarizability in a Single CdSe/ZnSe Quantum Dot. *Appl. Phys. Lett.* **2001**, *79*, 1033–1035.
20. Shirasaki, Y.; Supran, G. J.; Tisdale, W. A.; Bulovic, V. Origin of Efficiency Roll-Off in Colloidal Quantum-Dot Light-Emitting Diodes. *Phys. Rev. Lett.* **2013**, *110*, 217403.
21. Cognet, L.; Tsyboulski, D. A.; Rocha, J.-D. R.; Doyle, C. D.; Tour, J. M.; Weisman, R. B. Stepwise Quenching of Excion Fluorescence in Carbon Nanotubes by Single-Molecule Reactions. *Science* **2007**, *316*, 1465–1468.
22. Böhmler, M.; Hartmann, N.; Georgi, C.; Hennrich, F.; Green, A. A.; Hersam, M. C.; Hartschuh, A. Enhancing and Redirecting Carbon Nanotube Photoluminescence by an Optical Antenna. *Opt. Express* **2010**, *18*, 16443–16451.
23. Roslyak, O.; Cherqui, C.; Dunlap, D. H.; Piryatinski, A. Effect of Localized Surface-Plasmon Mode on Exciton Transport and Radiation Emission in Carbon Nanotubes. *J. Phys. Chem. B* **2014**, *118*, 8070–8080.
24. Htoon, H.; O'Connell, M. J.; Cox, P. J.; Doorn, S. K.; Klimov, V. I. Low Temperature Emission Spectra of Individual Single-Walled Carbon Nanotubes: Multiplicity of Subspecies within Single-Species Nanotube Ensembles. *Phys. Rev. Lett.* **2004**, *93*, 027401.
25. Galland, C.; Hoegele, A.; Tuereci, H. E.; Imamoglu, A. Non-Markovian Decoherence of Localized Nanotube Excitons by Acoustic Phonons. *Phys. Rev. Lett.* **2008**, *101*, 067402.
26. White, B.; Banerjee, S.; O'Brien, S.; Turro, N. J.; Herman, I. P. Zeta-Potential Measurements of Surfactant-Wrapped Individual Single-Walled Carbon Nanotubes. *J. Phys. Chem. C* **2007**, *111*, 13684–13690.
27. Sun, Z.; Nicolosi, V.; Rickard, D.; Bergin, S. D.; Aherne, D.; Coleman, J. N. Quantitative Evaluation of Surfactant-stabilized Single-walled Carbon Nanotubes: Dispersion Quality and Its Correlation with Zeta Potential. *J. Phys. Chem. C* **2008**, *112*, 10692–10699.
28. Moristubo, S.; Murai, T.; Shimada, T.; Murakami, Y.; Chiashi, S.; Maruyama, S.; Kato, Y. K. Exciton Diffusion in Air-Suspended Single-Walled Carbon Nanotubes. *Phys. Rev. Lett.* **2010**, *104*, 247402.
29. Xie, J.; Inaba, T.; Sugiyama, R.; Homma, Y. Intrinsic Diffusion Length of Excitons in Long Single-Walled Carbon Nanotubes from Photoluminescence Spectra. *Phys. Rev. B: Condens. Matter Mater. Phys.* **2012**, *85*, 085434.
30. Neuhauser, R. G.; Shimizu, K. T.; Woo, W. K.; Empedocles, S. A.; Bawendi, M. G. Correlation between Fluorescence Intermittency and Spectral Diffusion in Single Semiconductor Quantum Dots. *Phys. Rev. Lett.* **2000**, *85*, 3301–3304.
31. Mohite, A. D.; Gopinath, P.; Shah, H. M.; Alphenaar, B. W. Exciton Dissociation and Stark Effect in the Carbon Nanotube Photocurrent Spectrum. *Nano Lett.* **2008**, *8*, 142–146.
32. Bakker, H. J.; Bonn, M. Femtosecond Vibrational Spectroscopy of Aqueous Systems. In *Ultrafast Infrared Vibrational Spectroscopy*; Fayer, M. D., Ed.; CRC Press: Boca Raton, FL, 2013; pp 99−148.
33. Yoshikawa, K.; Matsunaga, R.; Matsuda, K.; Kanemitsu, Y. Mechanism of Exciton Dephasing in a Single Carbon Nanotube Studied by Photoluminescence Spectroscopy. *Appl. Phys. Lett.* **2009**, *94*, 093109.
34. Nguyen, D. T.; Voisin, C.; Roussignol, Ph.; Roquelet, C.; Lauret, J. S.; Cassabois, G. Excitonic Homogeneous Broadening in Single-Wall Carbon Nanotubes. *Chem. Phys.* **2013**, *413*, 102–111.
35. Sakashita, T.; Miyauchi, Y.; Matsuda, K.; Kanemitsu, Y. Plasmon-Assisted Photoluminescence Enhancement of Single-Walled Carbon Nanotubes on Metal Surfaces. *Appl. Phys. Lett.* **2010**, *97*, 063110.
36. Hong, G.; Tabakman, S. M.; Welsher, K.; Wang, H.; Wang, X.; Dai, H. Metal-Enhanced Fluorescence of Carbon Nanotubes. *J. Am. Chem. Soc.* **2010**, *132*, 15920–15923.
37. McDonagh, C.; Stranik, O.; Nooney, R.; MacCaith, B. D. Optimisation of Plasmonic Enhancement of Fluorescence for Optical Biosendor Applications. In *Metal-Enhanced Fluorescence*; Geddes, C. D., Ed.; John Wiley & Sons, Inc.: Hoboken, NJ, 2010; pp 139−160.
38. Tame, M. S.; McEnery, K. R.; Ozdemir, S. K.; Lee, J.; Maier, S. A.; Kim, M. S. Quantum Plasmonics. *Nat. Phys.* **2013**, *9*, 329–340.
39. Schuller, J. A.; Barnard, E. S.; Cai, W.; Jun, Y. C.; White, J. S.; Brongersma, M. L. Plasmonics for Extreme Light Concentration and Manipulation. *Nat. Mater.* **2010**, *9*, 193–204.
40. Arnold, M. S.; Green, A. A.; Hulvat, J. F.; Stupp, S. I.; Hersam, M. C. Sorting Carbon Nanotubes by Electronic Structure Using Density Differentiation. *Nat. Nanotechnol.* **2006**, *1*, 60–65.
41. Ghosh, S.; Bachilo, S. M.; Weisman, R. B. Advanced Sorting of Single-Walled Carbon Nanotubes by Nonlinear Density-Gradient Ultracentrifugation. *Nat. Nanotechnol.* **2010**, *5*, 443–450.
42. Muskens, O. L.; Giannini, V.; Sanchez Gil, J. A.; Gomez Rivas, J. Optical Scattering Resonances of Single and Coupled Dimer Plasmonic Nanoantennas. *Opt. Express* **2007**, *15*, 17736–17746.
43. Biagioni, P.; Huang, J.-S.; Hecht, B. Nanoantennas for Visible and Infrared Radiation. *Rep. Prog. Phys.* **2012**, *75*, 024402.